Journal of Japan Association for Earthquake Engineering, Vol. 25, No. 13, 2025
[Technical Paper (Translated Paper)]

VIBRATION CHARACTERISTICS OF STEEL-FRAMED HOUSE BASED ON LONG-TERM SEISMIC OBSERVATION RECORDS AND MICROTREMOR MEASUREMENT

Masafumi MORI[1], Shigeaki TOHNAI[2], Tomoki KOBASHI[3], Yoshimichi KAWAI[4], Asami KANAMORI[5] and Jun TOBITA[6]

[1] Member, Dr. Eng., Professor, Nagoya University, Nagoya, Japan,
mori.masafumi.d5@f.mail.nagoya-u.ac.jp
[2] Senior Manager, Nippon Steel Corporation, Tokyo, Japan,
tohnai.673.shigeaki@jp.nipponsteel.com
[3] Dr. Eng., Associate Professor, Chiba Institute of Technology, Chiba, Japan,
kobashi.tomoki@p.chibakoudai.jp
[4] M. Eng., Nippon Steel Texeng. Co., Ltd, Tokyo, Japan,
kawai.yoshimichi.jb@tex.nipponsteel.com
[5] M. Eng., Former Student, Nagoya University, Nagoya, Japan,
kanamori.asami.f4@s.mail.nagoya-u.ac.jp
[6] Member, Dr. Eng., Professor, Nagoya University, Nagoya, Japan,
tobita.jun.b0@f.mail.nagoya-u.ac.jp

ABSTRACT: In this paper, we examine the dynamic properties of an existing 3-story light-gauge steel-framed house based on the observation records obtained from seismic observations and microtremor measurement. As a result, it was concluded as follows. The first is that a decrease in the natural frequency and an increase in the damping constant, which are thought to be caused by earthquakes and aging, were observed. The second is that even within an earthquake, the natural frequency drops during periods of particularly large amplitude and then recovers. It is possible that this characteristic mainly depends on a reversible phenomenon such as friction between non-structural members. The third is that at the microtremor level, the natural frequency is higher and the damping constant is smaller than during the earthquake.

Keywords: *Steel-framed house, Transfer function, Natural frequency, Damping factor, Amplitude dependency*

1. INTRODUCTION

A light-gauge steel-framed house (referred to as a steel-framed house) is a typical example of a thin, lightweight steel structure, in which the frame materials of 2 × 4 frame wall structure are replaced with

surface-treated thin, lightweight steel panels with a thickness of approximately 1 mm. Steel-framed houses offer advantages such that construction period is shorter than that of reinforced concrete structures because of less on-site work and easier constructability, in which walls, floors, roofs, and other components of both their structural and nonstructural members are composed of factory-made framing and facing panels and can consequently be assembled on-site, and that the story shear force response during an earthquake is smaller because of their lightweight members.

Steel-framed houses were imported to Japan from the United States for use in temporary housing following the 1995 Great Hanshin-Awaji Earthquake Disaster. Thereafter, several R&D efforts[1)], including the establishment of a steel-framed house design method by the Steel-Framed House Subcommittee of the Steel Association, have been conducted. Moreover, appropriate legislation covering thin plate lightweight steel section construction has been developed. The Notice on Light Gauge Sheet Construction (Ministry of Land, Infrastructure, Transport and Tourism (MLIT) Notice No. 1641, 2001) was issued in 2001, which designated the steel-framed house as a new method of construction. This was subsequently revised in 2012 (MLIT Notice No. 1024, 2012). Consequently, restrictions on the number of floors were eased, and it became possible to build structures of 4 floors or less.

Previous studies on the steel-framed houses have focused on experimental and analytical studies at the component level. These include assessing the ultimate strength, determining resilience properties and the modeling, and determining damping performance and improving this performance. These studies established seismic design methods, increased the accuracy of analytical models, and improved seismic performance, for example[2)]. However, there have been few studies based on seismic observations on the actual characteristics of steel framed houses in use, which are focused on in this study.

Seismic observations and microtremor measurements are frequently conducted to clarify the dynamic characteristics of actual buildings [3)]. In particular, the microtremor measurement results in the Tokyo metropolitan district caused by the 2011 off the Pacific coast of Tohoku earthquake has been extensively analyzed. Kashima et al.[4)] comprehensively investigated natural frequencies and damping factors from observation records of eight S-structure buildings with 9–33 stories (four of which contained damping devices) and two RC buildings with 30 or more stories. They clarified the long-term characteristic changes and amplitude dependence during, before, and after the main shock of this earthquake. The result showed that in the RC structure, the natural period increased 15–30 % in the principal motion and did not recover to the initial value after the earthquake. Cracks in the structure were assumed to have caused this phenomenon. However, for a super high-rise steel structure, the change in natural frequency was only a few percent. The amplitude dependency was also smaller in the case of S structures, and the change of the properties between before and after the earthquake was smaller than those of RC structures. The damping factor exhibits less amplitude dependency and long-term variation in the S structure, and was more stable. In these examples, maximum story deformation angles tended to be less than 1/1000.

For examples of structures in addition to super high-rise buildings related to this study, Shinohara et al.[5)] demonstrated that trends similar to those in the super high-rise buildings described above were observable for a 14-story vibration-controlled steel office building based on seismic observations since 2003. Arakawa et al.[6)] described in detail the time and amplitude dependence of first- to third-order natural frequencies and damping factors and their changes before and after the main shock based on their seismic records and microtremor measurements of an 11-story steel building. And as the natural frequency decreased by approximately 10% owing to the main shock and did not return to the state before the earthquake, they suggested the possible reduction in the anchorage of the nonstructural members. Moreover, the variation in the natural frequency was clear from the relation between the response amplitude and the natural frequency during the main shock. However, compared to these high- to mid-rise structures, observation examples of low-rise steel buildings and structures with large response and deformation are scarce. Ikeda[7)] performed a shaking table experiment to demonstrate the change in the natural frequencies and damping factors of a 4-story steel building specimen during a major earthquake, and their relations to structural damage were also examined. Similar cases studying a 3-story RC building in a major earthquake have also been reported[8)]. Each of these cases include

detailed discussions of changes in natural vibration characteristics based on observation records. It is expected that variations in their characteristics will occur due to structural characteristics, response levels, vibration characteristics analysis methods, etc.

Examples of studies of vibration characteristics based on actual measurements of the steel-framed houses are scarce. Fukuwa et al.[9] performed microtremor measurements and vibration experiments to capture the amplitude dependence and changes in natural frequencies and damping factors of a 2-story detached steel-framed house during the construction phase. Consequently, they inferred that nonstructural members exerted a significant impact. In addition, Fukuwa et al.[10] also conducted similar research on other types of 3-story steel houses. These cases did not involve seismic observations or studies of long-term changes since completion.

Till date, no earthquake resistant design method has been legally specified for 3-story steel-framed houses. Examinations were conducted to apply the allowable stress design method. Therefore, to understand the vibration characteristics specific to steel-framed houses and confirm the validity of applying allowable stress design, continuous seismic observations of an existing 3-story steel-framed house (designed and built by NIPPON STEEL TEXENG) have been conducted since 2009. In addition to providing an overview of the subject building and seismic observation system, this study analyzed the response properties of the subject building during earthquakes. Further, we constantly measured the building for microtremors and compared with the analysis results of seismic observation records. Furthermore, we analyzed the long-term changes in vibration characteristics of the building based on several small and medium earthquakes since the completion of the building.

2. OUTLINE OF THE TARGET BUILDING AND SEISMIC OBSERVATION

2.1 Target building

The target building for the seismic observation is a company dormitory in Kimitsu City, Chiba Prefecture, Japan. It is a 3-story steel-framed building comprising a dwelling unit measuring approximately 48 m (East to West) and 8 m (South to North), with stair halls located at the east and west ends. It is comparatively lightweight and supported by a spread foundation on relatively hard soil. According to the "Earthquake Damage Estimation in Chiba" website[11], the construction site is located on a hilly terrain, with the engineering bedrock equivalent to an SPT N-value of 50 is approximately 5 m from the ground surface, and the average shear wave velocity at layers shallower than this is approximately 280 m/s. Both the plane and façade are not irregular. Shear walls with ceramic or reinforced gypsum board facings were installed along both directions. Using ceramic facing or structural plywood as the floor material, the floor panels were considered rigid against in-plane deformation. Consequently, it was inferred that on design, the rigid floor hypothesis held true. However, the rigid floor hypothesis is merely a design-based estimate, and has not been verified through measurements and observations. The shear walls on the upper and lower floors are connected via hold down clamps for the transmission of axial force. Notably, there are more openings, such as entrance and large window, with hanging partition wall, etc., in the longitudinal direction than in the span direction.

2.2 Seismic observation system

Seismographs were installed at three locations: on the G.L., the 2F, and the 3F. The seismographs installed on the 2F and 3F were placed within the duct space near the north side of the living room, which is located close to the center of the building. The G.L. seismograph was placed on an independent foundation at a small distance from the building on its north side. Figure 1 shows a plane view, a cross-section view, and the seismic observation points of the building. Further, Photo 1 indicates the seismograph installations (2^{nd} floor, G.L.). The installation location of the G.L. seismograph was deemed to exert minimal influence of the vibration of the building due to the results of microtremor measurements and to the building itself being lightweight. The E-catcher NEW compact seismograph from OYO Seismic Instrumentation Corp. was employed. The noise level was under 3 Gal (cm/s^2), the

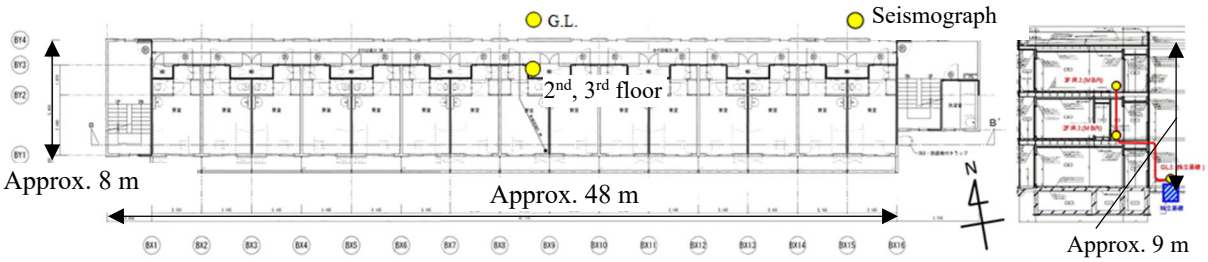

Fig. 1 Overview of the subject building and seismic observation points

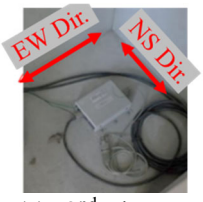

(a) 2nd Floor

(b) G.L.

Photo 1 Seismograph installations (2nd floor, G.L.)

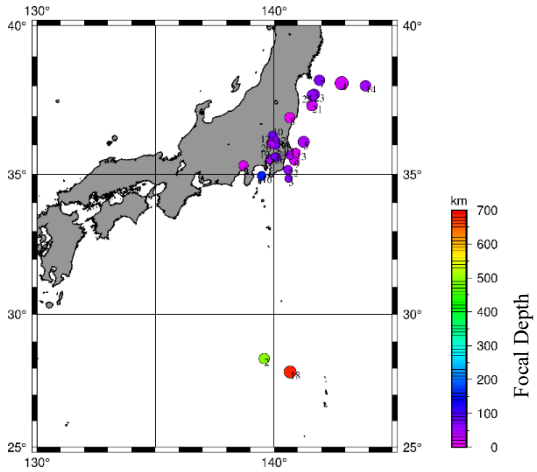

Fig. 2 Distribution of epicenters of seismic observation records

frequency range was DC to 20 Hz, and the sampling frequency was 100 Hz. Each seismograph was connected to a network and simultaneous observation could be undertaken. The trigger level for this observation was set to 5 Gal.

3. RESULTS OF ANALYSES BASED ON THE SEISMIC OBSERVATION RECORDS

3.1 Overview of observed seismic records

Observed seismic records are listed in Table 1. The distribution of epicenters of these seismic observation records is shown in Fig. 2.

Seismic observation records of 26 earthquakes were obtained within the period between the start of the observation and November 2022. The observation records comprised the main shock (No .4) and aftershocks (Nos. 7, 14, and 21) of the 2011 off the Pacific coast of Tohoku Earthquake. The seismic intensities (JMA) measured at the building sites were in the range of a high seismic intensity of under 5 which was observed during the 2011 off the Pacific coast of Tohoku Earthquake or lower to seismic intensity 2. In most cases, the seismic intensity was approximately 2 or 3. As examples of the observation records, based on the records with large maximum acceleration (instrumental seismic intensity), Fig. 3 shows the acceleration waveforms and tripartite spectra (damping factor is 5%) of (a) the 2011 off the Pacific coast of Tohoku Earthquake (No. 4), wherein the seismic motion lasted for a long-period with long-duration, and (b) the 2015 Tokyo Bay Earthquake (No. 19), which was a pulse type seismic motion having a predominantly short period. Estimated seismic intensities of above earthquakes at the building site were of under 5 and 3, respectively. Although (a) the 2011 off the Pacific coast of Tohoku Earthquake was larger in terms of seismic intensity, the 2015 Tokyo Bay Earthquake may have had a larger impact on the building response from the standpoint of the first natural frequency of the building at completion being 6–7 Hz (about 0.15 s) in the survey conducted before this measurement was performed.

Table 1 List of observed seismic records

記録番号	Eq. No.	Time		Location	Latitude	Longitude	Magnitude	Depth	Max. SI	PGA(EW) (cm/s^2)	PGA(NS) (cm/s^2)	SI (Site)	Epicenter distance
20	1	2009/11/14	4:23:36	Tokyo Bay	35°28.1′	139°47.7′	Mj 4.2	39 km	3	11.4	−18.4	2	16 km
21	2	2010/11/30	12:24:39	Off the western coast of the Ogasawara Islands	28°21.5′	139°35.3′	Mj 7.1	494 km	3	−7.0	8.0	2	775 km
22	3	2011/2/5	10:56:12	Off the southeast coast of Chiba Prefecture	34°51.3′	140°37.1′	Mj 5.2	64 km	4	−7.4	−5.2	2	87 km
01	4	2011/3/11	14:46:18	Off the coast of Sanriku	38°06.2′	142°51.6′	Mw 9.0	24 km	7	82.9	−68.0	5-	406 km
02	5	2011/3/11	15:15:34	Off the coast of Ibaraki Prefecture	36°07.2′	141°15.1′	Mj 7.6	43 km	6+	39.8	−33.7	4	152 km
03	6	2011/3/15	22:31:46	Eastern part of Shizuoka Prefecture	35°18.5′	138°42.8′	Mj 6.4	14 km	6+	−12.3	−12.9	3	106 km
04	7	2011/4/7	23:32:43	Off the coast of Miyagi Prefecture	38°12.2′	141°55.2′	Mj 7.2	66 km	6+	−6.4	7.1	2	367 km
05	8	2011/4/11	17:16:12	Hamadori, Fukushima Prefecture	36°56.7′	140°40.3′	Mj 7.0	6 km	6-	−9.1	−10.0	3	192 km
06	9	2011/4/12	8:08:16	Off the eastern coast of Chiba Prefecture	35°28.9′	140°52.0′	Mj 6.4	26 km	51	11.0	−13.5	3	91 km
07	10	2011/4/16	11:19:32	Southern Ibaraki Prefecture	36°20.4′	139°56.7′	Mj 5.9	79 km	5+	−14.7	−10.4	2	111 km
08	11	2011/4/21	22:37:02	Off the eastern coast of Chiba Prefecture	35°40.5′	140°41.1′	Mj 6.0	46 km	5-	7.2	6.6	2	82 km
09	12	2011/7/15	21:01:11	Southern Ibaraki Prefecture	36°09.8′	140°05.0′	Mj 5.4	66 km	5-	6.3	9.8	2	93 km
10	13	2012/3/14	21:05:04	Off the eastern coast of Chiba Prefecture	35°44.8′	140°55.9′	Mj 6.1	15 km	5+	8.4	8.7	2	106 km
11	14	2012/12/7	17:18:31	Off the coast of Sanriku	38°01.1′	143°52.0′	Mj 7.3	49 km	5-	−9.6	12.6	3	464 km
12	15	2013/11/10	7:37:51	Southern Ibaraki Prefecture	36°00.1′	140°05.0′	Mj 5.5	64 km	5-	10.0	−15.0	2	76 km
13	16	2014/5/5	5:18:25	Sea near Izu Oshima	34°57.1′	139°28.8′	Mj 6.0	156 km	5-	−43.2	−40.2	3	56 km
14	17	2014/9/16	12:28:32	Southern Ibaraki Prefecture	36°05.6′	139°51.8′	Mj 5.6	47 km	5-	−7.9	−6.7	2	84 km
15	18	2015/5/30	20:23:02	Off the western coast of the Ogasawara Islands	27°51.6′	140°40.9′	Mj 8.1	682 km	5+	28.6	19.4	4	833 km
16	19	2015/9/12	5:49:07	Tokyo Bay	35°33.2′	139°49.7′	Mj 5.2	57 km	5-	−53.1	33.4	3	24 km
17	20	2016/5/16	21:23:02	Southern Ibaraki Prefecture	36°02.0′	139°53.2′	Mj 5.5	42 km	5-	−7.4	6.3	2	77 km
18	21	2016/11/22	5:59:47	Off the coast of Fukushima Prefecture	37°21.2′	141°36.2′	Mj 7.4	25 km	5-	−7.2	7.9	3	272 km
19	22	2018/7/7	20:23:49	Off the eastern coast of Chiba Prefecture	35°09.9′	140°35.5′	Mj 6.0	57 km	5-	14.2	−21.3	3	68 km
31	23	2021/2/13	23:07:51	Off the coast of Fukushima Prefecture	37°43.7′	141°41.9′	Mj 7.3	55 km	6+	18.7	−11.3	3	312 km
32	24	2021/10/7	22:41:23	Northwestern part of Chiba Prefecture	35°35.4′	140°6.2′	Mj 5.9	75 km	5+	−50.5	33.1	4	35 km
33	25	2022/3/16	23:36:33	Off the coast of Fukushima Prefecture	37°41.8′	141°37.3′	Mj 7.4	57 km	6+	15.2	14.6	3	305 km
34	26	2022/3/31	20:52:14	Tokyo Bay	35°37.3′	140°1.9′	Mj 4.7	73 km	4	12.5	−11.6	3	35 km

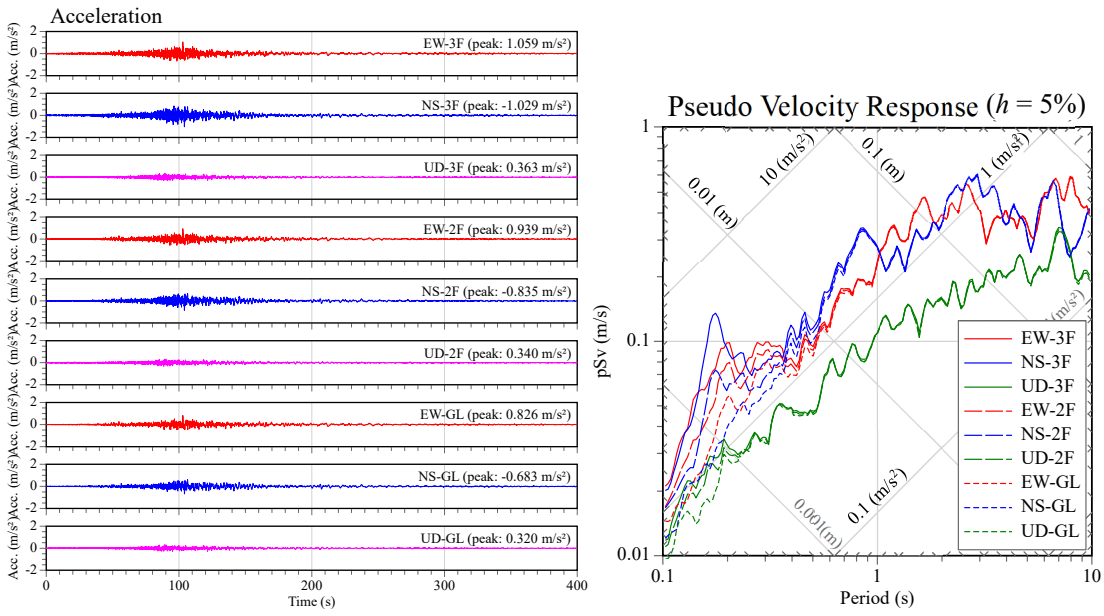

(a) The 2011 off the Pacific coast of Tohoku Earthquake (No. 4)

Fig. 3 Examples of observed seismic records (1 of 2)

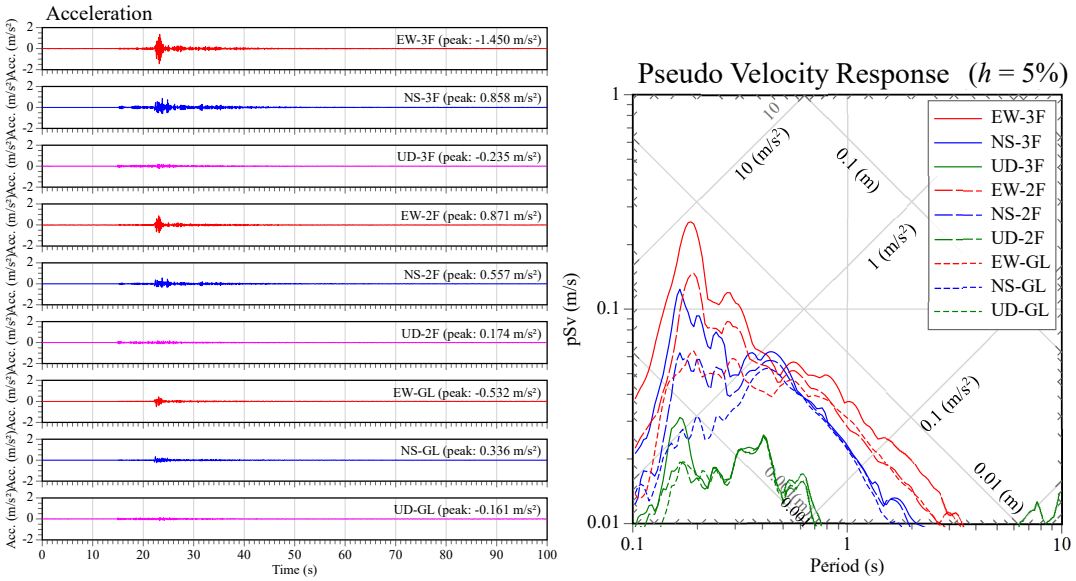

(b) 2015 Tokyo Bay Earthquake (No. 19)

Fig. 3 Examples of observed seismic records (2 of 2)

3.2 Comparison of maximum acceleration response distribution

The maximum acceleration response distribution, the lateral shear distribution factor A_i, etc. of all seismic observation records at the building are shown in Fig. 4. Figures 4(a)–4(b) present a comparison of (i) the maximum acceleration response, (ii) acceleration response ratio, (iii) equivalent A_iC_0, and (iv) A_i with the design values. Here, C_0 is the standard shear coefficient. The red lines in figures (i)–(iii) of Fig.4 indicate the results of earthquake No.4 and the blue lines indicate those of earthquake No. 19. Owing to the impossibility of setting up a seismograph on the rooftop, records were not obtained there. Therefore, when calculating (iii)–(iv) , it was assumed that the maximum acceleration on the rooftop was calculated via the addition of the average of the maximum acceleration increments of both from the 1F to the 2F and from the 2F to the 3F to the maximum acceleration at the 3F. Further, it was assumed that the mass of each floor was the same, and that of the rooftop was one-half of the other floors. The seismic hazard zoning factor Z and the design spectral factor R_t were assumed to be 1.0. We estimated the equivalent A_iC_0 ((iii)) by calculating the layer shear force based on the inertia force calculated from the maximum acceleration and mass of each floor, and subsequently dividing it by the weight above that layer. Moreover, in comparisons with the design value of A_i ((iv)), the equivalent A_iC_0 ((iii)) of each layer was standardized with that of the first layer. The green and purple lines in (iv) indicate A_i based on the approximate first natural frequency estimated from seismic records and that when using the first natural frequency employed in the design, respectively. Figure 5 shows a histogram of the average value of each floor acceleration response amplification ratio to G.L. Figure 6 presents the relationship of the base shear coefficient C_b to PGA. The base shear coefficient C_b used the value of the lowest layer of the equivalent A_iC_0 ((iii)). For more information about above parameters, refer to APPENDIX.

Figures 4(a)–4(b) exhibit the same trends (i) the maximum acceleration response distribution and (ii) acceleration response ratio distribution nearly uniform to inverted triangular form in both lateral directions, although under the condition when the rooftop records could not be obtained. Further, from (ii), it is recognized that the response amplitudes of the 3F to G.L. exhibited a range of approximately 1–4 times. In addition, there is different in the distribution shapes between the 2011 off the Pacific coast of Tohoku Earthquake (red line) which contained many long-period components and the Tokyo Bay Earthquake (blue line) which contained many short-period components. It presumably depends on the differences of the seismic input motion characteristics (spectral characteristics and maximum values) because the building is a lightweight low-rise building on good ground and the dynamic soil-structure interaction effect is small. Further, from (iii), it was estimated that the base shear

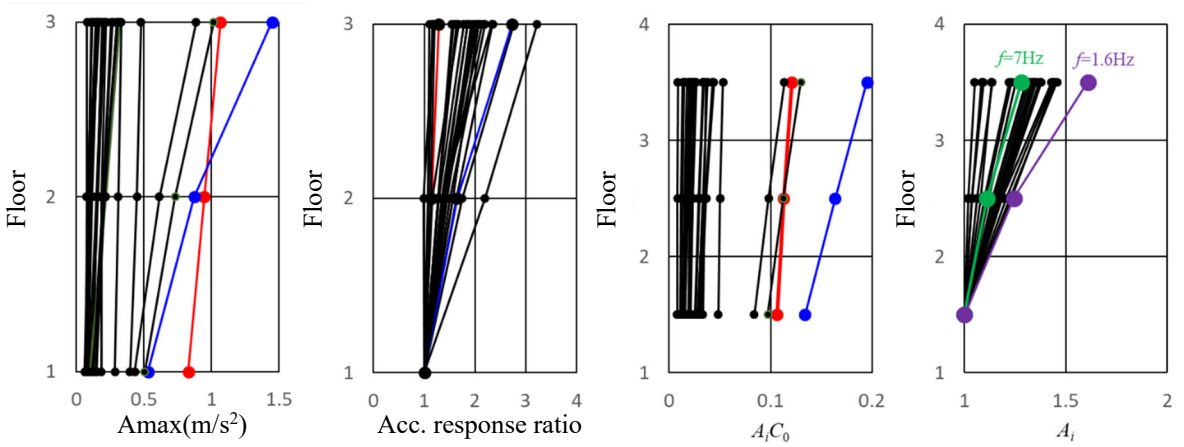

(i) Maximum acceleration response (ii) Maximum acceleration ratio (iii) Equivalent A_iC_0 (iv) A_i (green:observed, purple:design)

(a) EW direction

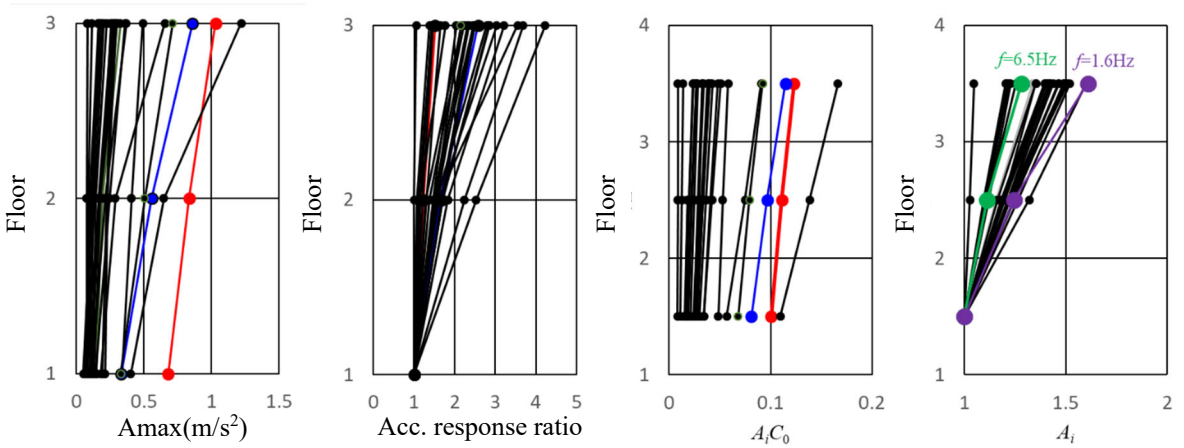

(i) Maximum acceleration response (ii) Maximum acceleration ratio (iii) Equivalent A_iC_0 (iv) A_i (green:observed, purple:design)

(b) NS direction

Fig. 4 Maximum acceleration response distributions and the lateral shear distribution factor A_i (in (1)–(3), red : earthquake No. 4, blue : earthquake No. 19)

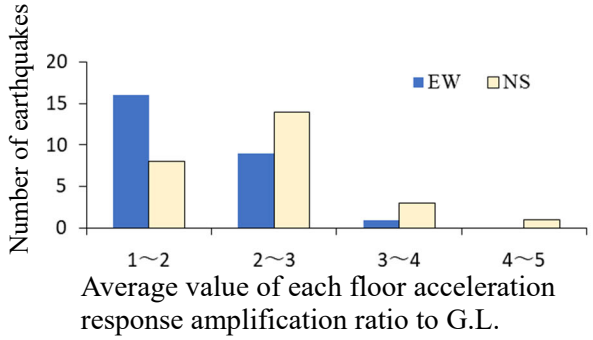

Fig. 5 Histogram of average value of each floor acceleration response amplification ratio to G.L.

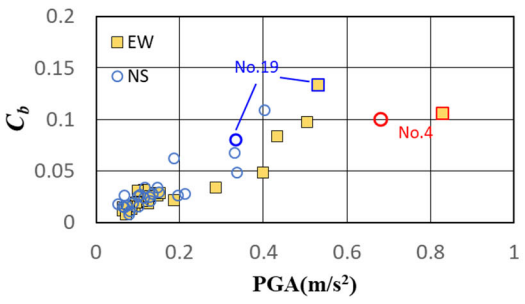

Fig. 6 Relationship of C_b to PGA

coefficient was a maximum of approximately 0.13 if the mass of each floor except the rooftop was maintained as constant. Moreover, in (iv), a large disparity in the distribution is evident. The A_i (green) using the first natural frequency estimated from the observation records was the average of A_i calculated from each observation record. On the other hand, the A_i (purple) using first natural frequency based on the design code was sufficient to encompass all earthquakes. Thus, using the first natural frequency of the design code, it can be said that the evaluation is on the safe side for the shear force distribution in the height direction. However, as in Fig. 5, the average value of each floor acceleration response amplification ratio to G.L. ranged as 1–5 times. Thus, the level of input acceleration of the seismic input motion for the same base shear differed by approximately 1/1 – 1/5. Consequently, there was a disparity in the base shear coefficient acting on the building for the same PGA, as shown in Fig. 6. Generally, although the PGA at C_b = 0.2 ranges as 0.8–1.0 m/s^2, extrapolation of the analysis results from these observation records suggested that the range was much wider. Thus, it must be considered that even when setting the A_i on the safe side, the assumed acceleration level of the seismic input motion may be relatively small. However, owing to the small dynamic interaction effect between the soil and the structure in the observed building, the sway mode may not be dominant in this building. Thus, the above range is considered to be primarily dependent on the periodic characteristics of seismic input motions.

3.3 Analysis using transfer functions

The natural frequencies and damping factors of the building were estimated using transfer functions. The transfer functions employed the H1 estimation method for estimation, which emphasizes the characteristics

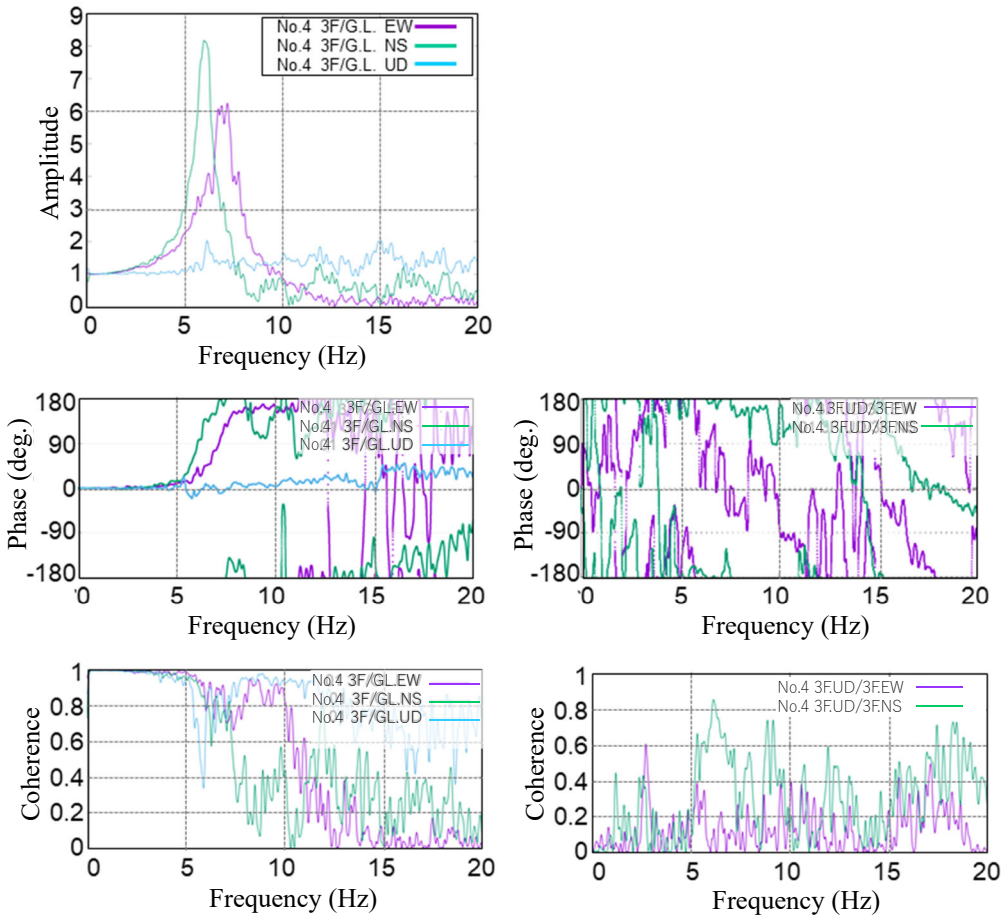

(a) 3F/G.L. (b) 3F–UD/3F–horizontal

Fig. 7 Transfer functions of 3F/G.L. in three direction and UD/Hor. at 3F (earthquake No.4)

of the frequency band in case of a large correlation between the two components[12]. Figure 7 shows transfer functions for Earthquake No .4. Figure 7(a) presents the transfer functions from G.L. to 3F in 3 directions and Fig. 7 (b) presents those between two horizontal directions on the 3F and UD direction on the same floor. Time synchronization of the seismographs is vital because the transfer function and spectral fitting used in this study also considered the frequency domain phase characteristics. In the records used in this study, time deviations were presented for each seismograph. Thus, time alignment was performed for each seismic record and directional component by focusing on the phase angle slope of the transfer function in the frequency domain wherein the correlation between the seismographs was high on the low-frequency side under the first natural frequency. We focused the analysis on the range below 10 Hz, wherein is large coherence is prevalent. As evident, the 3F/G.L. transfer functions in the EW and NS directions had clear peaks at approximately 7 and 6 Hz, respectively, with a slightly smaller peak at approximately 6 Hz in the UD direction. However, the effects of torsional vibration, including other earthquakes, were not clearly observable as the seismic observation points were set only at the center of the building plane. Torsional vibration and other three-dimensional vibration characteristics may be confirmed using the results of microtremor measurements. We will discuss about this for the future.

The horizontal and UD direction coherences shown in Fig. 7 (b) were particularly large in the vicinity of the peak frequencies of the NS and UD directions. There was a correlation between vibrations along these two directions. Further, the phase angle herein was approximately 180°. Considering that the seismograph was installed near the shear wall, this may be a coupled horizontal and vertical vibration caused by the rotation of the wall. However, it needs more additional analyses.

Next, natural frequencies and damping factors of the target building were estimated by the curve fitting method to transfer functions.

Referring to the study by Tobita[13], the curve fitting was performed for transfer functions (absolute value) in the EW and NS directions of 3F/G.L. while considering the effect of the horizontal orthogonal direction in the following equation.

$$J(\gamma) = \int_{\omega_1}^{\omega_2} \left| Z_{x_{obs}}(\omega) - Z_x(\gamma, \omega) \right|^2 d\omega \rightarrow \min \tag{1}$$

$$\begin{aligned} Z_x(\gamma,\omega) = & \left(\sum_{s=1}^{N} \frac{\omega^2 \beta_{sxx} u_{sx}}{\omega_{sx}^2 - \omega^2 + 2h_{sx}\omega_{sx}\omega i} + 1 \right) A_x(\omega) \\ & + \left(\sum_{s=1}^{N} \frac{\omega^2 \beta_{sxy} u_{sx}}{\omega_{sx}^2 - \omega^2 + 2h_{sx}\omega_{sx}\omega i} \right) A_y(\omega) \\ & + \left(\sum_{s=1}^{N} \frac{\omega_{sx}^2 + 2h_{sx}\omega_{sx}\omega i}{\omega_{sx}^2 - \omega^2 + 2h_{sx}\omega_{sx}\omega i} v_{sx} \right) + \left(\sum_{s=1}^{N} \frac{\omega_{sx}^2 \omega i}{\omega_{sx}^2 - \omega^2 + 2h_{sx}\omega_{sx}\omega i} d_{sx} \right) \end{aligned} \tag{2}$$

Here, γ: identification variables (= ω_{sx}, h_{sx}, β_{sxx}, β_{sxy}, v_{sx}, d_{sx}), ω: circular frequency, ω_{sx}: s-order natural circular frequency of the vibration component to be evaluated, h_{sx}: s-order damping factor of the vibration component to be evaluated, β_{sxx}: s-order participation factor of the vibration component to be evaluated, β_{sxy}: s-order participation factor of the orthogonal component of the vibration component to be evaluated, v_{sx}: initial value of s^{th} mode response velocity of the vibration component to be evaluated, d_{sx}: initial value of s-order mode response displacement of the vibration component to be evaluated, A_x: Fourier spectrum of the seismic input motion of the evaluated vibration component at G.L., A_y: Fourier spectrum of the input seismic motion in the orthogonal direction of the evaluated vibration component at G.L., N: number of modes to be considered in the model. This study assumed that a single-degree-of-freedom system (N = 1). And based on the signal-to-noise ratio of the observation records and the shape of the transfer function, f_1 (= $\omega_1/2\pi$) = 3 Hz and f_2 (= $\omega_2/2\pi$) = 10 Hz were set in Eq. (1). Additionally, with the addition of zeros to the before and after the waveform data, or the setting of the start and end

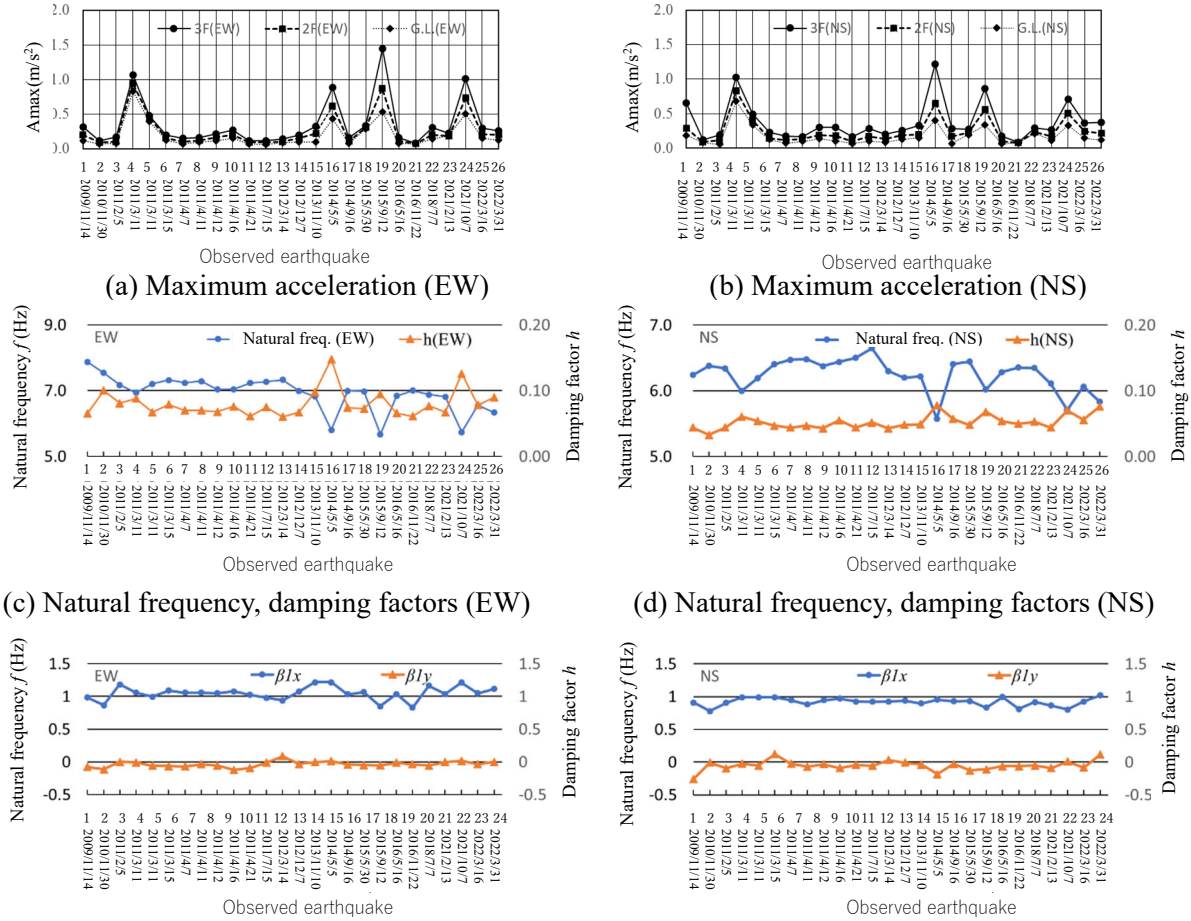

(a) Maximum acceleration (EW)

(b) Maximum acceleration (NS)

(c) Natural frequency, damping factors (EW)

(d) Natural frequency, damping factors (NS)

(e) Participation factors (EW)

(f) Participation factors (NS)

Fig. 8 Change trends of vibration characteristics associate with a series of earthquakes with different input levels

points of the data to zero via the taper process, v_{sx} and d_{sx} were given zero.

The maximum horizontal acceleration values at each floor, the estimated natural frequencies and damping factors are shown in Fig. 8 in order of the date when the earthquakes occurred. From Figs. 8(c)–8(d), the first natural frequencies were in the range of 5.7–7.9 Hz in the EW direction and 5.7–6.6 Hz in the NS direction. Further, the EW direction generally had higher values than the NS direction. Compared to the design natural frequency (period) [14] of the building, which was approximately 1.7 Hz (0.6 s), these values are large. When studying the application of allowable stress design to steel-framed houses, the stress-deformation relationship was studied by applying a static incremental analysis for a frame without nonstructural members. Further, the equivalent natural frequency of 1.7 Hz (0.6 s), which was estimated from the equivalent stiffness at a story deformation angle of approximately 1/300 based on the results, was employed as the natural frequency for design purposes. The story deformation angles of the building for the earthquakes treated in this analysis exhibited lower values than this (approximately 1/10000 – 1/4000). In the case of small and medium earthquakes, the effects of nonstructural members, which comprise face material the same as structural members, were also included. Therefore, it was inferred that the natural frequencies obtained from the earthquake observation records were large values compared to the first natural frequency for the seismic design. On the other hand, if earthquake Nos. 16, 19, and 24, which recorded larger accelerations than the other earthquakes, were excluded, the damping factors were approximately 6–10 % and 4–7 % in the EW and NS directions, respectively. which were similar to the design value[14] of 6 %.

Comparing the natural frequencies, it was found that the natural frequencies of the target building were similar to or slightly higher than those of the 2-story steel-framed house[9] with considering that the

height of the target building is higher than that of the 2-story house. Moreover, the natural frequencies of both horizontal directions were not sufficiently close to excite the torsional phenomenon as observed in the 2-story steel-framed house. In a similar manner, although the estimation method differed, the damping factors were similar at the time of building completion. However, considering that the damping factor of a typical S-structure building is 1–2 %, it can be concluded that the high damping factor is characteristic of the steel-framed house, which is composed of panels for walls, floors, and roofs.

In addition, when examining the relationship among these characteristics to the maximum acceleration ((a) and (b) of Fig. 8) on the 3F, the phenomenon wherein the first natural frequency decreased temporarily in an earthquake with a large maximum acceleration and subsequently returned to a value close to that before the earthquake with the large acceleration during the subsequent earthquake with the smaller maximum acceleration was observed. In contrast to this, damping factors exhibited a slightly increasing trend. This may be owing to certain reversible phenomena such as friction between nonstructural members, rather than damage to the structural members.

The target building was composed of thin sheet lightweight steel. Thus, it may be affected by rising temperatures during the summer months. When comparing the natural frequencies of Nos. 12 and 17 which occurred during the summer months (July–September) and exhibited similar intensity (intensity 2) to those of other earthquakes in other seasons, no significant difference was observed in this study.

The order of earthquake observation dates indicated that owing to the experience of earthquakes, the first natural frequency gradually decreased with age, and this trend as particularly notable in the EW direction (the longitudinal direction). However, although the damping factor appeared to increase slightly, no clear trend was observed. Based on the participation factors shown in (e) and (f), it was confirmed that the orthogonal component of the vibration (β_{1y}) exerted a very minimal influence.

Next, we investigated the amplitude dependence of the first natural frequency and the damping factor. Figures 9(a)–9(b) show the relationship between the maximum response acceleration, the natural frequencies and the damping factors. Figures 9(c)–9(d) show the relationship between the maximum relative displacement (from G.L. to 3F), the natural frequencies and the damping factors. For reference purposes, the plots corresponding to earthquake No. 4 and No. 19 are clearly indicated in the same figure. In terms of the natural frequency, a tendency for the natural frequency to decrease with increasing amplitude was observed. Although no clear trends were observed, the amplitude dependence was more significant in the EW direction. Meanwhile, despite the lack of a clear trend, the damping factors tended to increase slightly in the EW direction. The amplitude dependence of the damping factor was not clear in high-rise S-structures, for example [4), 5)]. Moreover, in the mid-rise structures' example [6)], the trend of amplitude dependence is observed at higher modes. This may depend on both of low-rise and the unique properties of the steel-framed house.

3.4 Time variation in the vibration characteristics during an earthquake

We analyzed the time variation of the vibration characteristics of the target building during an earthquake. Short time interval data were extracted from an observed acceleration record. Further, the H1 estimation method was used to calculate nonstationary transfer functions from these data. The interval start time was shifted by a fixed width to obtain nonstationary transfer functions. As the response amplification owing to long-period components below 2 Hz was considered to be small, the interval length and interval moving width were set to 5.12 and 0.1 s, respectively. A three-dimensional diagram depicting the nonstationary transfer function was drawn with the start time, frequency, and amplitude of the interval on each axis. Owing to space constraints, this study focused only on Earthquake No. 4 (the 2011 off the Pacific coast of Tohoku Earthquake, long duration), and Earthquake No. 19 (Tokyo Bay earthquake, short duration and pulse waveform), among the observed records with large amplitudes. In Section 3.3, these earthquakes exhibited smaller natural frequencies than the other earthquakes.

The results were shown in Fig. 10. A large decrease in the peak frequency was observed at the time of maximum amplitude in the EW direction of (b) Earthquake No. 19, which had a larger amplitude. This was followed by a gradual return to the original frequency (area circled by the red line). On the other hand, (a) Earthquake No. 4 exhibited a gradual decrease in the peak frequency and a tendency

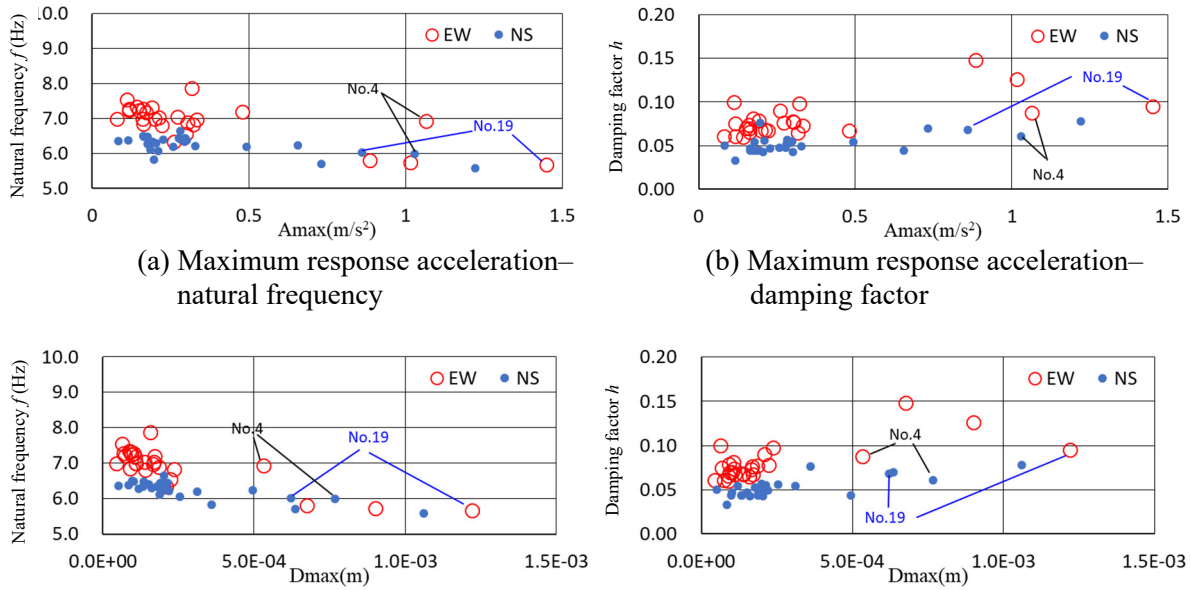

(a) Maximum response acceleration–natural frequency

(b) Maximum response acceleration–damping factor

(c) Maximum relative displacement–natural frequency

(d) Maximum relative displacement–damping factor

Fig. 9 Amplitude dependence of the first natural frequency and the damping factor

to return to the original value (circled in red); however, this was not as pronounced as that in case of (b) Earthquake No. 19.

Further, we investigated the amplitude dependence of the natural frequency and the damping factor during one earthquake. A curve fitting method was used to estimate the building's natural frequency and damping factor in each interval. The time window width and moving time for nonstationary transfer functions were set to 5.12 and 0.1 s, respectively. Fitting was performed by applying the least-squares approximation, while assuming a single-degree-of-freedom system for transfer functions (absolute value) in the EW and NS directions of 3F/G.L. for all time intervals. Considering the results of the previous analysis, the vibrational orthogonal component was disregarded. Further, the transfer function peaks may not be clearly expressed in certain intervals, such as at the beginning and end of the tremor and during large amplitudes. Therefore, the accuracy of the fitting was considered to be low in such intervals. Subsequently, we obtained the enveloping waveforms both of the absolute acceleration and the relative velocity waveforms at the 3F in order to determine the root mean square (RMS) value of the amplitude of time intervals of these waveforms [15]. When calculating the RMS value, the enveloping waveform was used to avoid the possibility of including a very short-period component with large amplitude in the recordings. This was because the time intervals were short, and thus the component could have a significant effect.

Figure 11 shows the relationship between the first natural frequencies and RMS values both of the absolute acceleration at the 3F and the relative velocity at the 3F with respect to G.L. In addition, the relationship between the damping factors and the relative velocity of the 3F with respect to G.L. is presented. The data after the 99th interval (9.9–15.02 s) are presented considering the pre-trigger between 15 s on the seismograph. Further, the data from the beginning of the tremor to the interval where the RMS value of the amplitude was the largest among all intervals are shown in blue, and the subsequent data are shown in orange. Notably, the intervals wherein the accuracy of the fitting was low, for instance where the optimal values could not be obtained, were the regions with small maximum absolute acceleration and maximum relative velocity values.

From these figures, it can be verified that the natural frequencies exhibited a downward trend to the right, thus amplitude dependence. The natural frequency in Earthquake No. 19 decreased significantly near the interval of maximum amplitude. However, in the subsequent interval, the natural frequency returned to a value close to that at the beginning of the tremor. In existing results for high-rise steel buildings e.g. [4), 5)], similar results were observed in the range where the amplitude was not excessively

large, although there are certain cases wherein the middle-rise steel building[6] did not return to its initial value. Thus, it is considered unlikely that the building would have severe structural damages by pulsed seismic input motion with a maximum acceleration of 140 Gal (Earthquake No. 19, EW direction). On the other hand, although large variations appeared in the damping factor, the damping factor tended to increase according to relative velocity increasing in the range where the relative velocity was approximately 0.2 cm/s or higher in the EW direction of (a) Earthquake No. 4. Similar trend was observed regarding the amplitude dependence of the vibration characteristics for the various earthquakes discussed in Section 3.3.

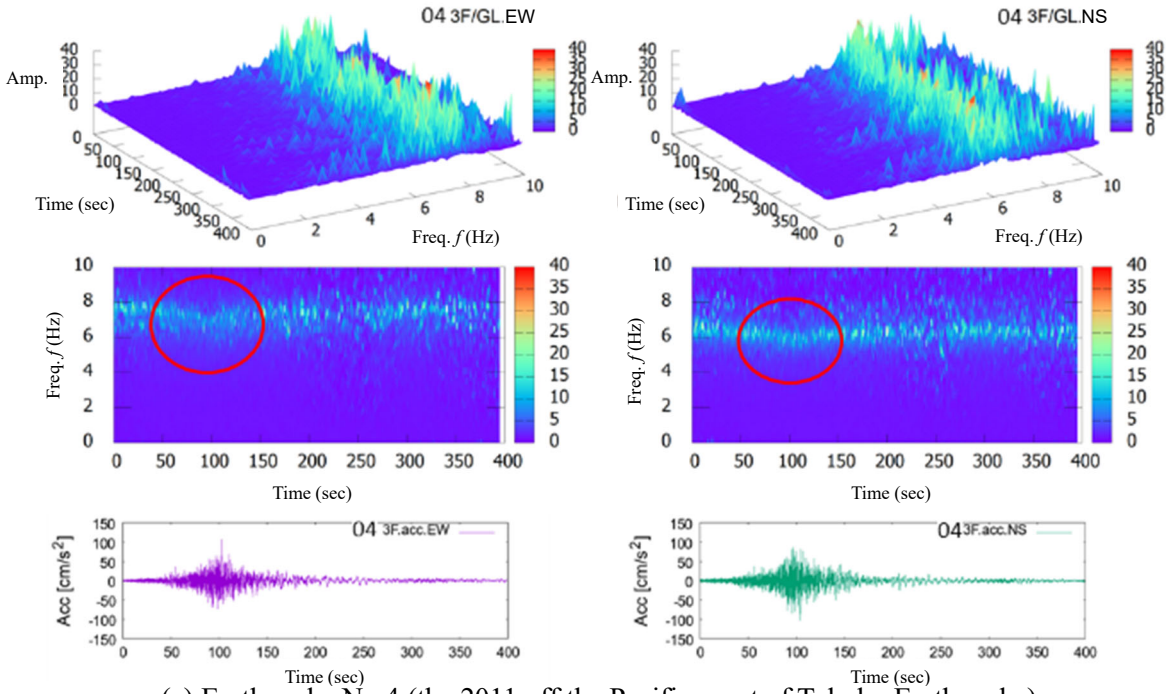

(a) Earthquake No.4 (the 2011 off the Pacific coast of Tohoku Earthquake)

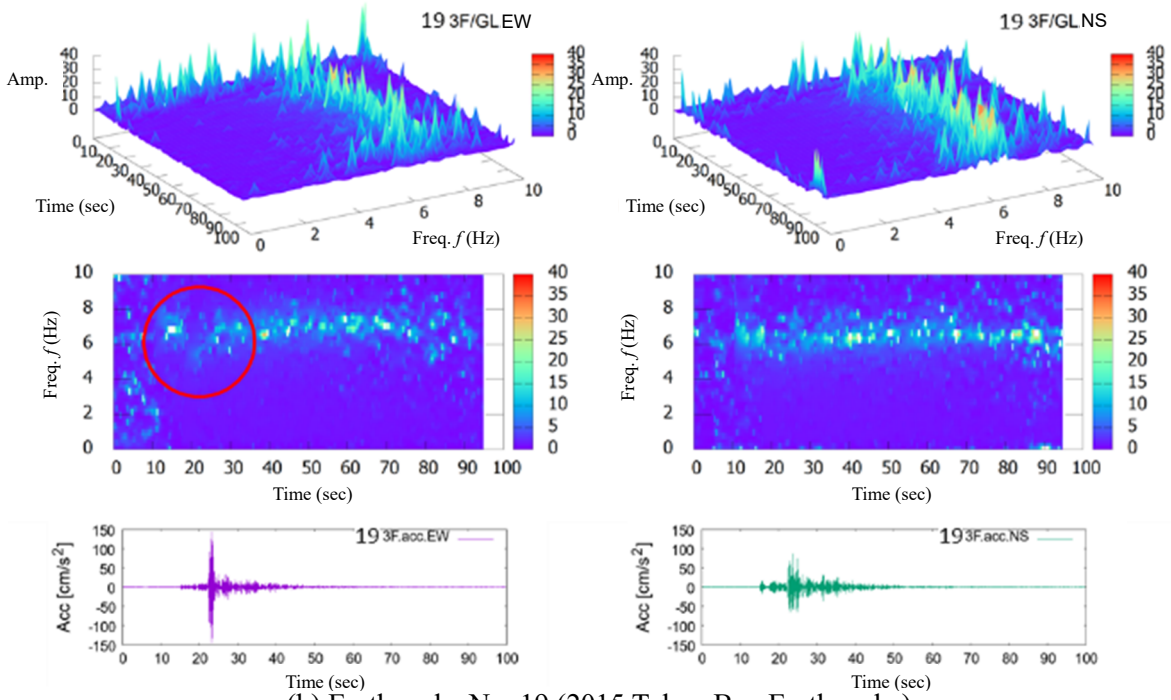

(b) Earthquake No. 19 (2015 Tokyo Bay Earthquake)

Fig. 10 Nonstationary transfer functions for two earthquakes

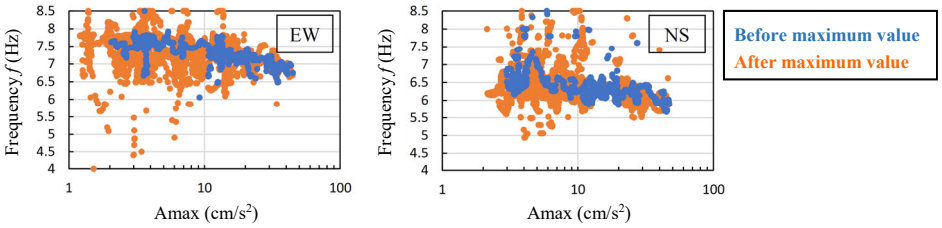

(i) Natural frequency – Maximum absolute acceleration

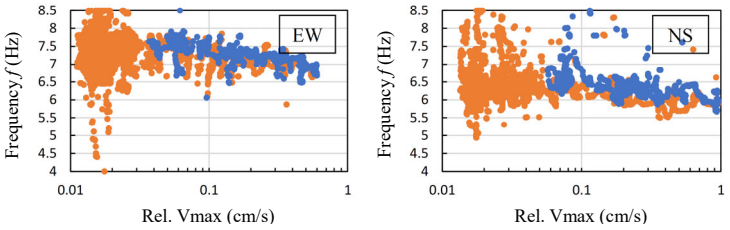

(ii) Natural frequency – Maximum relative velocity

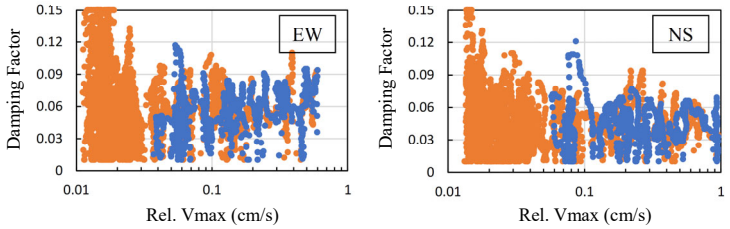

(iii) Damping factor – Maximum relative velocity

(a) Earthquake No.4 (the 2011 off the Pacific coast of Tohoku Earthquake)

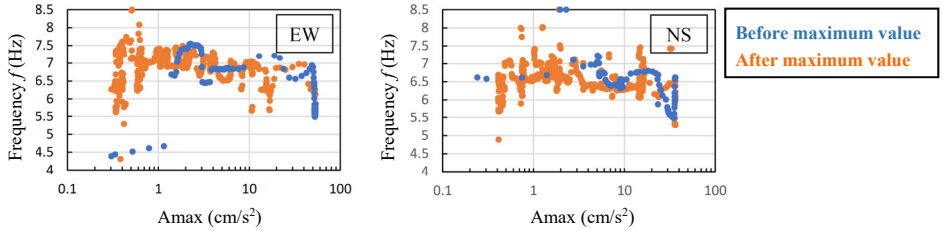

(i) Natural frequency – Maximum absolute acceleration

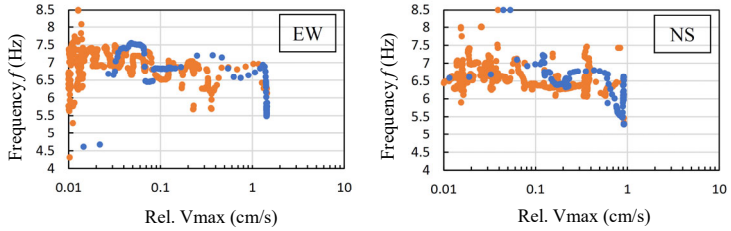

(ii) Natural frequency – Maximum relative velocity

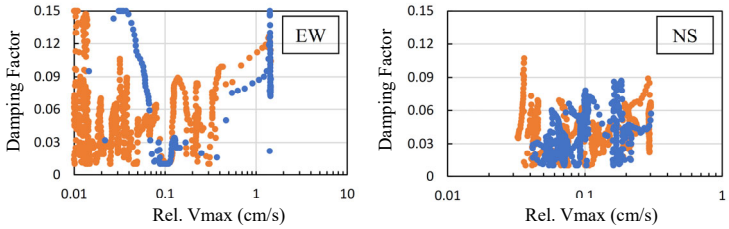

(iii) Damping factor – Maximum relative velocity

(b) Earthquake No. 19 (2015 Tokyo Bay Earthquake)

Fig. 11 Amplitude dependence of the first natural frequencies and damping factors in one earthquake

However, no significant trend appeared for (a) Earthquake No. 4 in the NS direction or (b) Earthquake No. 19. In addition, for (a) Earthquake No. 19 in particular, major differences and sharp drops even in the absolute acceleration and relative velocity of the same magnitude were recognized. Comparison with (b) Earthquake No. 4, the cause was inferred to be mainly stemming from seismic input motion characteristics. As shown in Fig. 10, this earthquake exhibited a pulsed seismic waveform. Therefore, under the pulsed seismic input motion, slippage between the components occurred and the vibration frequency changed rapidly when the building response exceeded a certain amplitude level and the frictional force acting between the structural members exceeded the static frictional resistance. Moreover, it is considered that the differences in the direction of the earthquake are also primarily owing to the difference in the envelope shape of the seismic wave.

4. VIBRATION PROPERTIES ANALYSIS BASED ON MICROTREMOR MEASUREMENTS

This chapter presents the results of the analysis of microtremor measurements of the target building, etc., conducted in October 2022.

4.1 Overview of microtremor measurements

Microtremor measurements were conducted at three buildings: two steel-framed houses of the same size built simultaneously on the same site (in this case, SE and SW buildings), in addition to the target building wherein the earthquake observation was conducted (here, the N building). Measurements were performed twice, once in the N building and once in the SE and SW buildings. Further, one reference point (C–gr) was placed on the free ground surface approximately 15 m south of the west edge of the N building, which was approximately halfway between the S and N buildings. Microtremor measurements were conducted at the N building in 2009 when the building was completed. Here, we describe the results of the analysis of the N building, wherein seismic observations were also conducted. Figure 12 shows the observation system for microtremor measurement at the N building. Owing to the building being currently used as a company dormitory, the measuring points were placed in the areas that would not interfere with its usage, such as vacant rooms. The measurement device used was a JU410 made by HAKUSAN Corp. Each measurement lasted for 1 hour, and they were acquired on October 6, 2022 (weather: rain).

4.2 Results

Transfer functions for the 3F (N_03cc) to the G.L. (grnc) located on the side of the N building are shown in Fig. 13. Transfer functions for the 3F (N_03cc) to the free ground surface (C–gr) of the N building are shown in Fig. 14. From these figures, although the peak frequencies and values differed slightly depending on the ground stations used in the analysis, the differences are approximately 1–5 % for the frequency and 10 % for the peak value, the impact of the differences in the stations was small. The results of the curve fitting method using the same method as described above are indicated by red lines in the same figures. Although there were two peaks in the transfer functions in the NS direction, there was a clear peak at the higher frequency with the Fourier spectrum of the 3F. Moreover, as the dynamic soil-structure interaction effect is small, this peak was judged to be the natural frequency of the N building. The peak at the low frequency can be partly attributed to the very small amplitude component at the frequency in the denominator of the microtremor record at the free ground surface.

The natural frequency and damping factor obtained via the curve fitting method superimposed on top of Fig. 8 are shown in Fig. 15. The results of the microtremor measurements performed at the time the building was completed (March 2009) are also presented in Fig. 15. From these results, both the natural frequencies and damping factors decreased compared to those when the building was completed. Compared with the obtained seismic observation records, the natural frequencies were higher and the damping factors were lower than the values during the earthquakes. Moreover, the decrease in the natural frequency appears to be larger in the EW direction.

From the above discussion, it can be inferred that, in addition to aging deterioration, the contact surfaces between nonstructural members, and between the steel frame and plasterboard, may have loosened

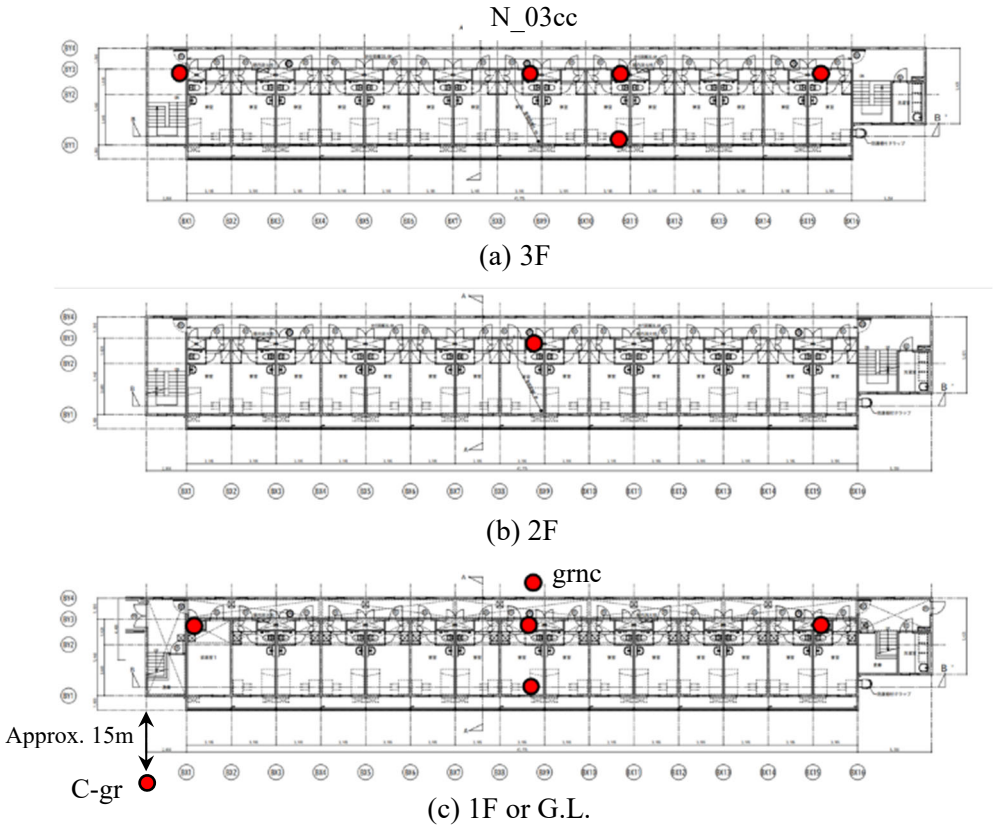

(a) 3F

(b) 2F

(c) 1F or G.L.

Fig. 12 Observation points for microtremor measurement in the N Building

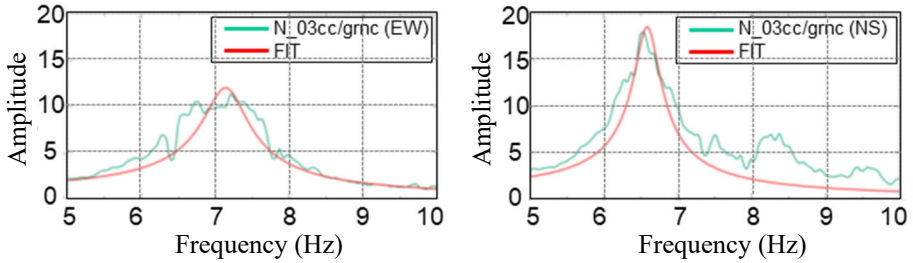

(a) EW direction (b) NS direction

Fig. 13 Transfer function for the 3rd floor (N_03cc) to the G.L. (grnc) of near the N building

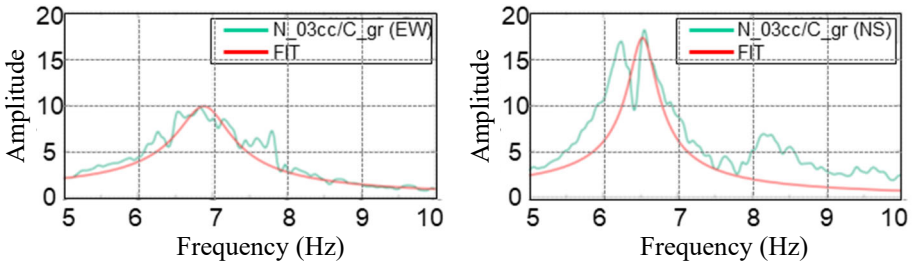

(a) EW direction (b) NS direction

Fig. 14 Transfer function for the 3F (N_03cc) to the free ground surface (C–gr) of the N building

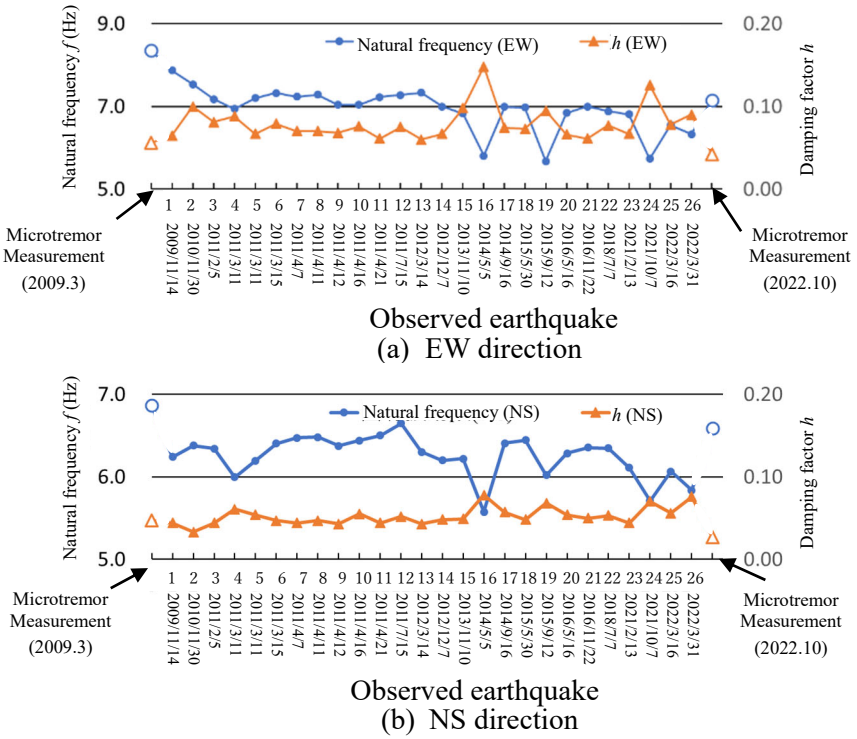

Fig. 15 Changes in natural frequencies and damping factors in the N Building from March 2009 to October 2022 (Microtremor measurement results added to Fig. 8.)

owing to the occurrence of multiple earthquakes since construction completion, although they were mostly small and medium earthquakes, thereby resulting in a decrease in the natural frequency and damping factor at the microtremor level. The same tendency was observed in a previous study[9] on a 2-story detached house with a steel-framed house. However, in that case, the vibration conditions were different. Moreover, Nakata et al.[16] analyzed the changes in dynamic characteristics caused by building components such as interior materials and ALC walls for a lightweight steel building. They suggested that building parts may contribute to stiffness at small amplitudes; however, these have little effect at large amplitude levels. The damping factor was also larger with larger amplitude levels. Similar characteristics were indicated by the results of the present analysis.

We performed a visual inspection of the external appearance of the structure while measuring microtremors. However, no cracks, which were conclusively judged to be caused by earthquakes were observed. To confirm this point, the changes of the natural frequency and the damping factor during one earthquake, particularly during the initial and subsequent motions, as shown in Fig. 11, should be carefully analyzed for all earthquakes, in addition to continued observation.

5. CONCLUSION

This study examined the vibration characteristics of a steel-framed house and its change owing to earthquakes, based on the results of long-term seismic observations conducted over a period of approximately 13 years. Further, microtremor measurements conducted both after the completion of construction and at present were investigated. The results showed a decrease in the natural frequency and an increase in the damping factor. This may be owing to the effects of earthquakes and aging. The natural frequency of the steel-framed house was lower than the design value (A_i was over-estimated), and the damping factor was approximately the same as the design value. In addition, the results of analyzing the changes in vibration characteristics (amplitude dependence) during one earthquake using nonstationary transfer functions revealed a decrease in natural frequency during the period of particularly large amplitude that occurs during one earthquake which later recovers. However, owing to

the large disparity in the data, a further in-depth study is required.

Moreover, from microtremor measurements, the results indicated that the natural frequency was higher at the microtremor level than at the seismic level. Whereas, the damping factor was slightly lower than at the time of completion of the construction. In future, these points must be analyzed quantitatively. Moreover, the effects of the above-mentioned changes on the seismic performance (strength, hysteresis damping, etc.) of the building must also be investigated. Thus, this study examined the seismic observation records at the center of a regular building and concluded that the rigid floor hypothesis and torsional vibrations exerted minimal effects. The validity of the rigid floor assumption and the effects of torsional vibration will be future works of this research.

APPENDIX: THE CURRENT JAPANESE SEISMIC DESIGN CODE PUBLISHED IN 1981

In relation to Section 3.2, the current Seismic Design Code of buildings in Japan published in 1981 defined the lateral seismic shear Q_i of the i-th story shown as in Eq. (A1).

$$Q_i = Z \cdot R_t \cdot A_i \cdot C_0 \cdot \sum_{j=i}^{N} w_j \tag{A1}$$

Here, Z : the seismic hazard zoning factor, R_t : the design spectral factor, A_i : the lateral shear distribution factor, C_0 : the standard shear coefficient, w_j : weight at the jth floor, N: the number of floors.

REFERENCES

1) Kawai, Y., Kanno, R., Uno, N. and Sakumoto, Y. : Seismic Resistance and Design of Steel-Framed Houses, *Nippon Steel Report*, No. 369, pp. 8–17, 1998 (in Japanese).
2) Takeuchi, T and Marukawa, T. : Damping Properties of Bearing Walls of Steel-Framed Housings– Dynamic Behavior of Wall Panel with Finishing and Effect of Additional Dampers, *Journal of Structural and Construction Engineering*, The Architectural Institute of Japan, Vol. 615, pp. 181–188, 2007 (in Japanese).
3) Tobita, J., Kashima, T., Nakamura, M., Uetake, T., Yamamura, K., Kurita, K. and Kambara, H. : Database of Earthquake Response Observation of Buildings in Japan, *AIJ Journal of Technology and Design*, Vol. 20, No. 46, pp. 901–904, 2014 (in Japanese).
4) Kashima, T., Koyama, S., Azuhata, T. and Inoue, N. : Change in Dynamic Characteristics of Super High-Rise Buildings due to the 2011 Great East Japan Earthquake, *AIJ Journal of Technology and Design*, Vol. 21, No. 48, pp. 493–497, 2015 (in Japanese).
5) Shinohara, T. and Kazuma, H. : Earthquake Records of Nikken Sekkei Tokyo Building Following The 2011 off the Pacific Coast of Tohoku Earthquake Part 2: Overall Evaluation of the Records from April, 2003 to February, 2012, *Summaries of Technical Papers of Annual Meeting*, Architectural Institute of Japan, Structure II, pp. 1151–1152, 2012 (in Japanese).
6) Arakawa, T., Taniguchi, R., Nakamura, N., Kinoshita, T. and Tojo, T. : Evaluation of Vibration Characteristics Considering Higher Modes During Earthquakes for a Middle-Rise Steel Building, *Journal of Structural and Construction Engineering*, The Architectural Institute of Japan, Vol. 80, No. 717, pp. 1657–1666, 2015 (in Japanese).
7) Ikeda, Y. : Building Dynamic Property Change under an Earthquake Evaluated by the Forgetting Factor Recursive Least Squares Method, *AIJ Journal of Technology and Design*, Vol. 18, No. 38, pp. 51–54, 2012 (in Japanese).
8) Tobita, J., Takita, M., Moro, M. and Ito, K. : Change and Variation of Vibration Characteristics of a Low-Rise RC Building Subjected to Strong Ground Motions, *Journal of Structural Engineering*, Vol. 45B, pp. 73–80, 1999 (in Japanese).
9) Fukuwa, N., Nishizaka, R., Takahashi, H., Nakamura, H., Tobita, J. and Kawai, Y. : A Study on Dynamic Characteristics of a Steel-House Based on Vibration Tests, *Proceedings of the 10th Japan*

Earthquake Engineering Symposium, Vol. 2, pp. 1599–1604, 1998 (in Japanese).
10) Fukuwa, N., Tanaka, K. and Kondo, M. : A Study on the Eigenproperty of 3 Story Steel House Based on Vibration Test, *Journal of Structural Engineering*, Vol. 41B, pp. 279–287, 1995 (in Japanese).
11) Chiba Prefecture: Earthquake Damage Estimation in Chiba Website, (in Japanese). http://keihatsu.bousai.pref.chiba.lg.jp/higaisoutei/detail2/mapindex/index.html (last accessed on September 20, 2023)
12) Theoretical Earthquake Motion Research Society eds., *Seismic Motion—Synthesis and Waveform Processing—*, Kajima Institute Publishing Co., Ltd., 256 pp., 1994 (in Japanese).
13) Tobita, J. : Evaluation of Nonstationary Damping Characteristics of Structures under Earthquake Excitations, *Journal of Wind Engineering and Industrial Aerodynamics*, Vol. 59, No. 2–3, pp. 283–298, 1996.
14) Nippon Steel: Structural Calculations Sheet (3-Story Steel-Framed Houses Measured in this Paper), 2008 (in Japanese) .
15) Hirai, T. and Fukuwa, N. : Synthesis Method of Sound Which Has Same Duration Time as a Seismogram, *Zishin*, 2nd ed., Vol. 63, No. 3, pp. 153–163, 2011 (in Japanese).
16) Nakata, S., Kiriyama, S., Naito, S., Yoshida, A. and Tamura, Y. : Change of Dynamic Properties of Low-Rise Houses with Its Structural Components (Part 1) Online of Experiment, (Part 2) Experiment Results, *Summaries of Technical Papers of Annual Meeting*, Architectural Institute of Japan, Structure II, pp. 1001–1004, 2010 (in Japanese).

(Original Japanese Paper Published: February, 2024)
(English Version Submitted: April 17, 2025)
(English Version Accepted: August 8, 2025)